The instability of Wilton ripples

Olga Trichtchenko[1]†, Bernard Deconinck[2] and Jon Wilkening [3]

[1]Department of Mathematics, University College London, Gower Street, London, WC1E 6BT, UK

[2]Department of Applied Mathematics, University of Washington, Seattle, WA 98195-3925, USA

[3]Department of Mathematics and Lawrence Berkeley National Laboratory, University of California, Berkeley, CA 94720-3840, USA

(Received xx; revised xx; accepted xx)

Wilton ripples are a type of periodic traveling wave solution of the full water wave problem incorporating the effects of surface tension. They are characterized by a resonance phenomenon that alters the order at which the resonant harmonic mode enters in a perturbation expansion. We compute such solutions using non-perturbative numerical methods and investigate their stability by examining the spectrum of the water wave problem linearized about the resonant traveling wave. Instabilities are observed that differ from any previously found in the context of the water wave problem.

1. Introduction

In 1915 J. R. Wilton (Wilton 1915) included the effects of surface tension and constructed a series expansion in terms of the amplitude of one-dimensional periodic waves in water of infinite depth, extending Stokes's work (Stokes 1847). He noticed that if the (non-dimensionalized) coefficient of surface tension equals $1/n$ ($n \in \mathbb{Z}^+$), the Stokes expansions giving travelling wave solutions to Euler's equations are singular. As a way to rectify the problem, he modified the form of the perturbation expansion so that the nth harmonic enters at order $(n-1)$ or $(n-2)$ instead of n. The resulting solutions are known as resonant harmonics or Wilton ripples.

The occurrence of Wilton ripples is not merely a mathematical phenomenon. Henderson and Hammack (Henderson & Hammack 1987) generated and observed such waves in a controlled tank experiment. In the experiment, several sensors were placed at different points along the length of the tank. They measured the wave profile and the frequencies of the wave as it travelled down the tank. Even though waves of roughly 20Hz were generated by the paddles at one end of the tank, frequencies around 10Hz were observed as well. This is a manifestation of Wilton ripples.

McGoldrick contributed significantly to the understanding of gravity-capillary waves and their relation to resonant interaction, using both experiment and theory. He demonstrated experimentally that gravity-capillary waves lose their initial profile as they propagate (McGoldrick 1970*a*). He also examined these waves using weakly nonlinear theory (McGoldrick 1970*b*) and used the method of multiple scales (McGoldrick 1971) to investigate the evolution of the gravity-capillary waves. Further, resonant phenomena such as Wilton ripples have been studied in model equations. For instance Boyd and Haupt (Haupt & Boyd 1988) investigated Wilton ripples in the context of the so-called super Korteweg-de Vries or Kawahara (Kawahara 1972) equation by adding resonant harmonics into the series expansion, following Wilton's original approach (Stokes 1847).

† Email address for correspondence: o.trichtchenko@ucl.ac.uk

Akers and Gao (Akers & Gao 2012) derived an explicit series solution for the Wilton ripples in this same context.

Not much work has been done analyzing the stability of Wilton ripples. In fact, we are aware only of the work of Jones (Jones 1996, 1992). He investigated a system of coupled partial differential equations describing up to cubic order the interaction of the fundamental mode of a gravity-capillary wave with its second harmonic. He also provided wave train solutions of these equations. These were used to examine the stability of gravity-capillary waves as different parameters are varied. We will analyze the stability of resonant solutions by looking at the stability eigenvalue problem obtained by linearizing around a steady state solution. This was previously done by McLean (1982) (McLean 1982) who built on numerical work of Longuet-Higgins (Longuet-Higgins 1978*a*,*b*) as well as others to examine growth rates of instabilities as a function of wave steepness. We will also use the ideas seen in MacKay and Saffman (1986) (MacKay & Saffman 1986) and use the Hamiltonian structure of the problem in order to find where instabilities can occur.

In this paper, working with fully nonlinear solutions of the water wave equations, we investigate the spectral stability of resonant gravity-capillary waves using the Fourier-Floquet-Hill method (Deconinck & Kutz 2006). To our knowledge, our work presents the first study of the different instabilities to which Wilton ripples are susceptible, without restricting the nature of the disturbances. Our paper follows the previous investigations on the instabilities of one-dimensional periodic travelling gravity waves (Deconinck & Oliveras 2011) and of gravity waves in the presence of weak surface tension (Deconinck & Trichtchenko 2014). More details and a more comprehensive investigation of the different types of solutions, their series expansions, and their instabilities will be published elsewhere (Trichtchenko *et al.* 2015).

2. Computing Resonant Gravity-Capillary Waves

One-dimensional gravity-capillary waves are governed by the Euler equations,

$$\phi_{xx} + \phi_{zz} = 0, \qquad (x,z) \in D, \tag{1a}$$

$$\phi_z = 0, \qquad z = -h,\ x \in (0,L), \tag{1b}$$

$$\eta_t + \eta_x \phi_x = \phi_z, \qquad z = \eta(x,t),\ x \in (0,L), \tag{1c}$$

$$\phi_t + \frac{1}{2}\left(\phi_x^2 + \phi_z^2\right) + g\eta = \sigma \frac{\eta_{xx}}{\left(1+\eta_x^2\right)^{3/2}}, \qquad z = \eta(x,t),\ x \in (0,L), \tag{1d}$$

which incorporate the effects of both gravity and surface tension, where g is the acceleration due to gravity and σ is the coefficient of surface tension. Here h is the height of the fluid when at rest, $\eta(x,t)$ is the elevation of the fluid surface and $\phi(x,z,t)$ is the velocity potential. As was shown in (Vasan & Deconinck 2013), we can add an arbitrary function $C_\phi(t)$ (of time but not space) to the Bernoulli condition (1d), which we will do for computational purposes below. We focus on solutions on a periodic domain $D = \{(x,z) \mid 0 \leqslant x < L, -h < z < \eta(x,t)\}$ as shown in figure 1. It is clear that the parameter space for the travelling-wave solutions of this problem is extensive. A comprehensive investigation will be presented in (Trichtchenko *et al.* 2015). In this brief communication, we restrict our attention to solutions for which $g = 1$, the period $L = 2\pi$ and the water depth $h = 0.05$. If one employs the criteria of (Benjamin 1967; Benjamin & Feir 1967; Whitham 1967), this puts us in the shallow water regime, quite different from Wilton (Wilton 1915) who worked with $h = \infty$. However, it should be noted that

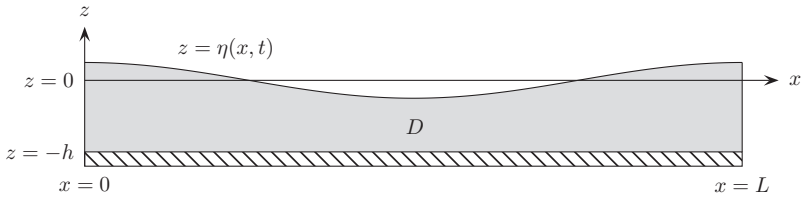

FIGURE 1. The domain on which we solve Euler's equations.

the above references distinguishing shallow water from deep water do not incorporate surface tension, and as such their results do not immediately apply.

The regular perturbation expansion (or Stokes expansion) for a 2π-periodic travelling water wave takes the form

$$\eta(x) = \epsilon \cos x + \sum_{k=2}^{\infty} \epsilon^k \eta_k(x), \quad \eta_k(x) = \sum_{j=2}^{k} 2\hat{\eta}_{kj} \cos(jx), \tag{2}$$

where the Euler equations are reduced using the travelling wave reduction $\partial_t \to -c\partial_x$. Regular perturbation theory (see, for instance, (Vanden-Broeck 2010)) leads to an expression for $\eta_k(x)$ with a denominator proportional to the left-hand side of

$$(g + \sigma)k \tanh(h) - \left(g + k^2\sigma\right) \tanh(kh) = 0, \qquad (k \neq 1). \tag{3}$$

We refer to (3) as the resonance condition as it indicates that the k-th harmonic is resonant with the base mode. If resonance occurs, *i.e.* (3) holds for a certain value of k, say $k = K$, the regular Stokes expansion breaks down, and it is not possible to determine $\eta_K(x)$ in the form (2). Instead, the resonant harmonic arises in the Stokes series at order ϵ^{K-1} or ϵ^{K-2} (Vanden-Broeck 2010; Wilton 1915). It is easy to see that (3) cannot hold when $\sigma = 0$. In other words, surface tension is a necessary condition for the occurrence of resonance. Further, (3) holds for at most one value of $k \geqslant 2$ (Trichtchenko *et al.* 2015).

To compute travelling solutions of (1a-d), we developed a variant of the boundary integral method of Wilkening & Yu for the time-periodic problem (Wilkening & Yu 2012), modified to take advantage of the travelling wave assumption. Considering only the equations (1c-d), which are valid at the surface $z = \eta$, and defining a surface velocity potential $q(x,t) = \phi(x, \eta(x,t), t)$, we have

$$-c\eta_x = \phi_z - \eta_x\phi_x := G(\eta)q, \tag{4a}$$

$$-cq_x = P\left[-c\phi_z\eta_x - \frac{1}{2}\left(\phi_x^2 + \phi_z^2\right) - g\eta + \sigma\frac{\eta_{xx}}{\left(1+\eta_x^2\right)^{3/2}}\right]. \tag{4b}$$

Here (4b) is obtained from (1d) by using $q_t = \phi_t + \phi_z\eta_t$ at the free surface prior to restricting to a travelling frame. Equation (4a) defines the Dirichlet to Neumann operator $G(\eta)$. Further, P is the projection operator onto functions of zero mean: $Pf(x) = f(x) - \frac{1}{2\pi}\int_0^{2\pi} f(x)dx$. The introduction of this operator is required since the left-hand side of (4b) clearly has zero average. This amounts to including $C_\phi(t)$ in (1d) to avoid secular growth in $\phi(t)$ as the wave travels. In addition, in the next step we invert $G(\eta)$. Working with functions of zero average guarantees the existence of a unique inverse.

As written, (4a-b) is a system of two equations for the two unknown surface variables $q(x)$ and $\eta(x)$, linked by $\phi(x,z)$ through the solution of Laplace's equation (1a) in the domain D. We solve the first equation for $q(x)$ using the inverse $G(\eta)^{-1}$ of the Dirichlet

to Neumann operator (Craig & Sulem 1993):

$$q = -cG(\eta)^{-1}\eta_x, \qquad \begin{pmatrix}\phi_x\\ \phi_z\end{pmatrix} = \frac{1}{1+\eta_x^2}\begin{pmatrix}1 & -\eta_x\\ \eta_x & 1\end{pmatrix}\begin{pmatrix}q_x\\ -c\eta_x\end{pmatrix}. \tag{5}$$

This determines q, ϕ_x and ϕ_z on the free surface given η. Equation (4b) may then be rewritten as $R(c,\eta)=0$, with

$$R(c,\eta) := P\left[c\phi_x - \frac{1}{2}\phi_x^2 - \frac{1}{2}\phi_z^2 - g\eta + \sigma\partial_x\left(\frac{\eta_x}{(1+\eta_x^2)^{1/2}}\right)\right], \tag{6}$$

where we moved cq_x inside $P[\cdots]$ and used $q_x = \phi_x + \phi_z\eta_x$. Next we define the objective function $F(c,\eta) = \frac{1}{4\pi}\int_0^{2\pi} R(c,\eta)^2\,dx$, which is minimized (holding the first Fourier mode of η fixed at the desired amplitude, $\hat{\eta}_1 = \epsilon/2$) using the modified Levenberg-Marquardt method developed by Wilkening and Yu in (Wilkening & Yu 2012).

Rather than computing the operator $G(\eta)$ as described in (Wilkening & Yu 2012) and inverting it in (5), we reverse the algorithm to directly compute the Neumann to Dirichlet operator. In more detail, $G(\eta)q$ can be computed by first solving a second-kind Fredholm integral equation $\left[\frac{1}{2}\mathbb{I}+\mathbb{K}\right]\mu = q$ to find the dipole density μ, and then evaluating $G(\eta)q = \left[\frac{1}{2}H+\mathbb{G}\right]\mu'$, where H is the Hilbert transform. Formulas for $\mathbb{K}$ and $\mathbb{G}$ are given in (Wilkening & Yu 2012). The modification is to solve $\left[\frac{1}{2}H+\mathbb{G}\right]\mu' = -c\eta_x$ for μ', which is essentially a second-kind Fredholm integral equation due to $H^2 = -P$; take an antiderivative to find μ; and evaluate $q = \left[\frac{1}{2}\mathbb{I}+\mathbb{K}\right]\mu$. The improved accuracy comes from taking an antiderivative instead of a derivative in the middle step. A similar idea was used by Sethian and Wilkening (Sethian & Wilkening 2004) in the context of linear elasticity to avoid loss of digits when evolving a semigroup whose generator involves two spatial derivatives of a type of Dirichlet-Neumann operator — the inverse operator can be computed much more accurately.

Figure 2 displays laptop-computed solutions running compiled `C++` code implementing the method sketched above. We use as many Fourier modes as needed to ensure the highest modes decay to double or quadruple-precision roundoff thresholds. A key difference between these numerical results and those for gravity waves with a small coefficient of surface tension (Deconinck & Trichtchenko 2014) is that the Fourier modes no longer decay monotonically. The solutions computed here show a resonance at the $K = 10$th mode and its higher harmonics. As the amplitude is increased, the modes neighboring the resonant modes start to grow as well.

3. Stability

We examine the stability of the solutions of the previous section using the Fourier-Floquet-Hill numerical method described in (Deconinck & Kutz 2006). Convergence theorems for this method are found in (Curtis & Deconinck 2010; Johnson & Zumbrun 2012). Denoting one of the travelling solutions computed above by $(\eta_0; q_0)$, we consider a perturbed solution

$$\eta(x,t) = \eta_0(x-ct)+\delta\eta_1(x-ct)e^{\lambda t}+\ldots, \qquad q(x,t) = q_0(x-ct)+\delta q_1(x-ct)e^{\lambda t}+\ldots. \tag{1}$$

Here $(\eta_1; q_1)$ is the spatial part of the perturbation, bounded for all x, including as $|x|\to\infty$. Specifically, $\eta_1(x)$ is not required to be periodic with the same period as $\eta_0(x)$. Note that $\mathrm{Re}(\lambda) > 0$ implies exponential growth of the perturbed solution, and thus instability of $\eta_0(x)$. Substitution of (1) in the governing equations (1a-d) and neglecting terms of order δ^2 yields a linear (but nonlocal) generalized eigenvalue problem for η_1, q_1 that is

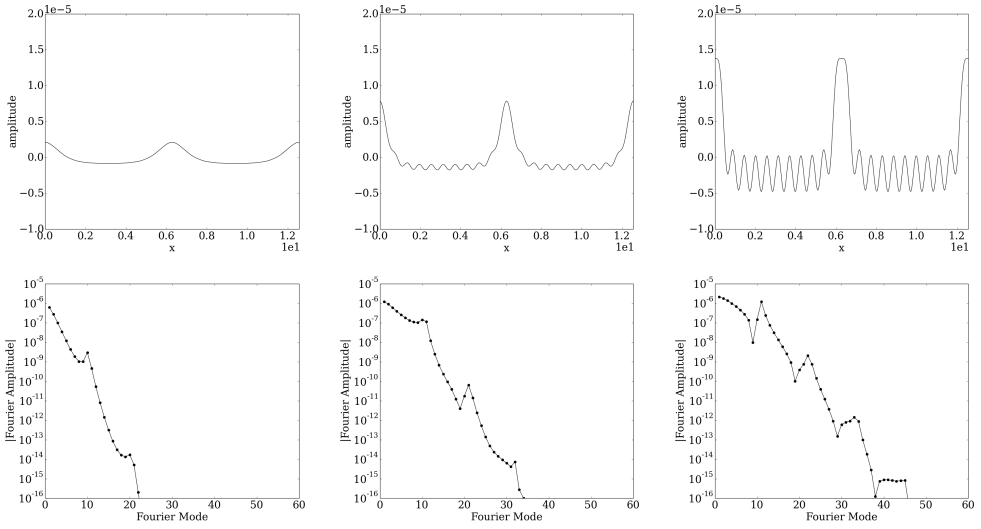

FIGURE 2. Wave profiles for solutions with amplitude $\epsilon = 2\hat{\eta}_1 = 1.244 \times 10^{-6}$, 2.448×10^{-6} and 4.254×10^{-6} (top), and semi-log plots of the absolute values of their Fourier modes $\hat{\eta}_k$ (bottom). Here $\hat{\eta}_k = \frac{1}{2\pi} \int_0^{2\pi} \eta(x) e^{-ikx}\, dx$. As expected from the results for gravity waves (Deconinck & Oliveras 2011), the troughs get wider and the crests become more narrow as the amplitude increases. The Wilton ripples also become more apparent, especially in the troughs. For the wave of highest amplitude plotted, a depression is present in the crest.

invariant under spatial translation by 2π; see (Deconinck & Oliveras 2011; Deconinck & Trichtchenko 2014). Therefore we expect η_1, q_1 to also be eigenfunctions of the shift operator, and hence be of Bloch form

$$\begin{pmatrix} \eta_1(x) \\ q_1(x) \end{pmatrix} = e^{i\mu x} \sum_{m=-\infty}^{\infty} \begin{pmatrix} \hat{N}_m \\ \hat{Q}_m \end{pmatrix} e^{imx} = \sum_{m=-\infty}^{\infty} \begin{pmatrix} \hat{N}_m \\ \hat{Q}_m \end{pmatrix} e^{i(m+\mu)x}, \qquad \mu \in (-1/2, 1/2]. \quad (2)$$

Due to the Hamiltonian nature of (1a-d) (Zakharov 1968), the spectrum of this generalized eigenvalue problem is reflection symmetric with respect to both the real and imaginary axes (Wiggins 1990). As a consequence, the presence of any eigenvalue λ off the imaginary axis implies instability.

For the case of flat water ($\eta_0(x) \equiv 0$), the spectrum may be computed analytically. It consists of all values of the form

$$\lambda^{\pm}_{\mu+m} = ic(\mu+m) \pm i\sqrt{[g(\mu+m) + \sigma(\mu+m)^3] \tanh((\mu+m)h)}, \;\; \mu \in (-1/2, 1/2], \; m \in \mathbb{Z}, \quad (3)$$

where $c = \sqrt{(g+\sigma)\tanh h}$ is the wave speed in the linearized regime. Since these values are all imaginary, we conclude that flat water is spectrally stable. However, as we examine solutions with a nonzero amplitude, instabilities arise. Figures 3 and 4 show detailed stability results for the three larger-amplitude solutions of figure 2. Figure 3 shows the complex λ plane, while figure 4 shows $\mathrm{Re}(\lambda)$ vs μ. Many phenomena are similar to those observed for gravity (Deconinck & Oliveras 2011) and (non-resonant) gravity-capillary (Deconinck & Trichtchenko 2014) waves, such as the presence of bubbles of high-frequency instabilities for the larger-amplitude waves. New phenomena are observed as well. We observe nested structures for the two larger-amplitude waves, and, despite being in shallow water, we notice the presence of a modulational instability (columns 2 and 3). As shown in the right panel of figure 5, the onset of this modulational instability

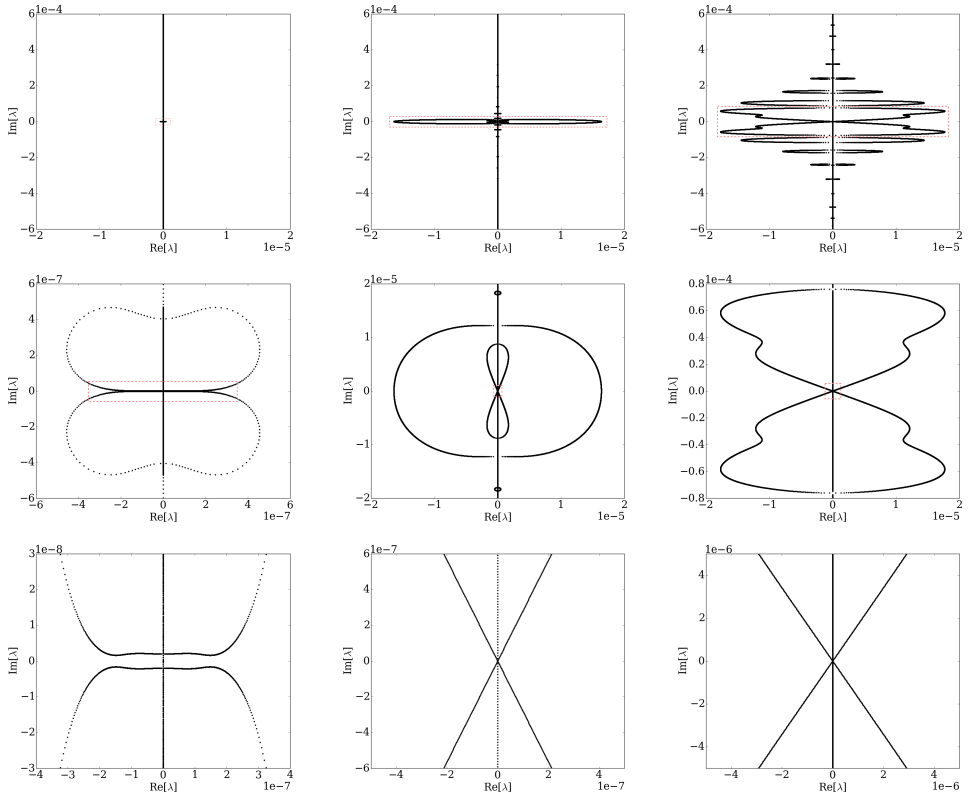

FIGURE 3. Stability results for the solutions shown in figure 2. The columns correspond to $\epsilon = 1.244 \times 10^{-6}$, 2.448×10^{-6}, and 4.254×10^{-6}, respectively. For each amplitude, two zooms of the region indicated by the red box above are presented in the second and third rows.

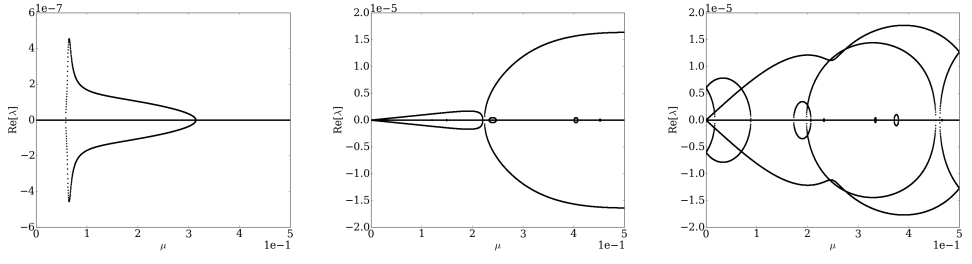

FIGURE 4. Dependence of $\mathrm{Re}(\lambda)$ on μ for $\epsilon = 1.244 \times 10^{-6}$, 2.448×10^{-6}, and 4.254×10^{-6}.

occurs around $\epsilon = 1.555 \times 10^{-6}$, when the large bubble of instability present at that amplitude merges with its mirror image at the origin.

Since eigenvalues are continuous with respect to variations of the wave amplitude (Hislop & Sigal 1996), eigenvalues may leave the imaginary axis as the amplitude increases only through collisions on the imaginary axis. This is required to ensure the Hamiltonian symmetry of the spectrum. Thus, a necessary condition for the loss of stability of $\eta_0(x)$ as the solution bifurcates away from the flat water state is that there exist μ and m such that one of the following conditions holds:

$$\lambda_\mu^+ = \lambda_{\mu+m}^+, \qquad \lambda_\mu^+ = \lambda_{\mu+m}^-, \qquad \lambda_\mu^- = \lambda_{\mu+m}^+, \qquad \lambda_\mu^- = \lambda_{\mu+m}^-. \tag{4}$$

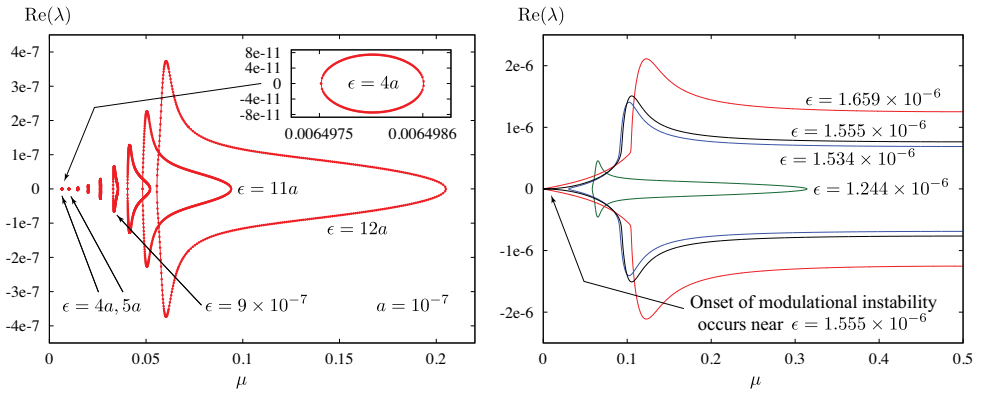

FIGURE 5. (left) Two bubbles of instability nucleate from the origin and move away from the Re(λ) axis in opposite directions as ϵ increases from 0. The second bubble (with $\mu < 0$) is not shown as the figure is reflection symmetric about $\mu = 0$ (and also about $\mu = 1/2$, by periodicity). (right) At larger amplitudes, the bubble merges with its mirror image to the right, and later with its image to the left, at the origin.

For the resonant solutions with $K = 10$, we have a six-way crossing at $\lambda = 0$ when $\mu = 0$, namely

$$\lambda_{\mu}^{+} = \lambda_{\mu}^{-} = \lambda_{\mu-1}^{+} = \lambda_{\mu+1}^{-} = \lambda_{\mu-10}^{+} = \lambda_{\mu+10}^{-} = 0, \qquad (\mu = 0). \tag{5}$$

To show that $\lambda_{\mu-10}^{+} = 0$ and $\lambda_{\mu+10}^{-} = 0$, the resonance condition (3) may be used in (3). As shown in figure 5, two bubbles of instability nucleate at this six-way crossing. As the wave amplitude ϵ increases away from zero, these instability bubbles leave the origin in the Re(λ) vs μ plane in opposite directions, one to the right (shown in figure 5), and the other to the left, a mirror image of the one to the right. For small values of ϵ, the bubbles are supported on intervals well separated from the origin. Indeed, the range of values μ over which we observe an eigenvalue λ with Re(λ) $\neq 0$ has the form $(-\mu_{1,\epsilon}, -\mu_{0,\epsilon}) \cup (\mu_{0,\epsilon}, \mu_{1,\epsilon})$, with $0 < \mu_{0,\epsilon} < \mu_{1,\epsilon} < 1/2$. Although $\mu_{0,\epsilon}$ and $\mu_{1,\epsilon}$ both approach zero as $\epsilon \to 0^{+}$, the width $\mu_{1,\epsilon} - \mu_{0,\epsilon}$ of each interval is much smaller than the gap $2\mu_{0,\epsilon}$ between intervals. For example, in the inset of the left panel of figure 5, when $\epsilon = 4 \times 10^{-7}$, the width is 1.09×10^{-6} while the gap is 11900 times larger. Thus, even though the instability nucleates at $\mu = 0$, it is not modulational since the wave numbers of the unstable perturbations are tightly confined to a narrow interval separated from the origin. In the right panel of figure 5, we see that as ϵ increases, the bubble grows in size, merges with its reflection about $\mu = 1/2$, and eventually forms a protrusion that connects with its reflection about $\mu = 0$ at the origin (around $\epsilon = 1.555 \times 10^{-6}$). Beyond this point, modulational instabilities are present.

We finish these preliminary stability considerations by examining the short-time effect of these instabilities on the water wave profiles they perturb. Given an eigenvalue-eigenfunction pair, the short-time dynamics of the perturbed wave profile is dictated by the linearized problem obtained above. We have

$$\eta(x + ct, t) \approx \eta_0(x) + \delta\,\mathrm{Re}\{e^{i\theta} e^{\lambda t} \eta_1(x)\}, \qquad \eta_1(x) = \sum_{m=-M}^{M} \hat{N}_m e^{i(m+\mu)x}, \tag{6}$$

where M is the number of Fourier modes of the computed eigenfunction and $\theta \in (-\pi, \pi]$ is an arbitrary phase; see (Deconinck & Kutz 2006; Deconinck & Oliveras 2011). Since the eigenfunction corresponding to $\bar{\lambda}$ (associated with $-\mu$) is the complex conjugate of

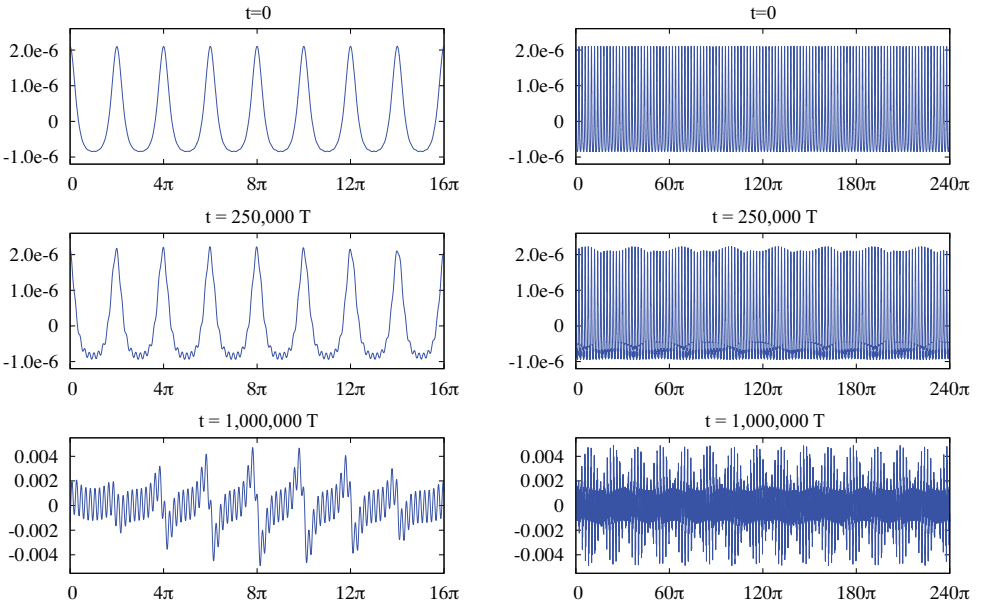

FIGURE 6. Three snapshots of a perturbation of the wave in the left column of figure 2 (with amplitude $\epsilon = 1.244 \times 10^{-6}$), approximated by (6) and plotted over 8 (left) or 120 (right) periods of the wave. Here $\mu = 0.06496517$ corresponds to the most unstable eigenvalue, namely $\lambda = (4.557154 + 2.322777i) \times 10^{-7}$, and $T = 2\pi/c = 28.09599$ is the time it takes the underlying traveling wave to traverse its wavelength. The unperturbed solution is in the resonant regime, but with secondary oscillations indiscernible since many periods are shown at once.

$\eta_1(x)$, $\mathrm{Re}(e^{\lambda t}\eta_1(x))$ and $\mathrm{Re}(ie^{\lambda t}\eta_1(x))$ span the same space as $e^{\lambda t}\eta_1(x)$ and $e^{\bar{\lambda} t}\overline{\eta_1(x)}$. If $\mathrm{Re}(\lambda) \neq 0$, Hamiltonian symmetry implies that $-\lambda$ and $-\bar{\lambda}$ are also eigenvalues, and the eigenfunctions can be obtained by reversing the sign of q (i.e. reversing time) and reflecting space. However, we focus here on linearized solutions that grow as $t \to +\infty$ rather than decay. The eigenfunctions (η_1, q_1) are normalized so that $\sum_{|m|\leqslant N} |\hat{N}_m|^2 = 1$, with complex phase chosen so that $\hat{N}_0$ is real and positive. The Fourier modes of the eigenfunctions are found to decay exponentially, so it is not difficult to resolve a given eigenfunction to double-precision accuracy.

Figure 6 shows the results of seeding the traveling solution $\eta_0(x - ct)$ of amplitude $\epsilon = 1.244 \times 10^{-6}$ with a multiple of the most unstable eigenfunction. This travelling wave corresponds to the left panels of figures 2, 3 and 4. From the results of figure 4, $\mathrm{Re}(\lambda)$ is maximized at $\mu = 0.06496417$ by $\lambda = (4.557154 + 2.322777i) \times 10^{-7}$. The approximation (6) was used with $\theta = 0$ and $\delta = \epsilon/200$. With the above normalization $\sum_m |\hat{N}_m|^2 = 1$, we have

$$\|\eta_1\|_\infty = \max_{0\leqslant x\leqslant 2\pi} |\eta_1(x)| = 2.159, \qquad \|\delta\eta_1\|_\infty / \|\eta_0\|_\infty = 0.00639.$$

The left column of figure 6 shows eight periods of the traveling wave while the right column shows 120 periods. In both columns, $\eta(x + ct, t)$ is plotted, showing the results in a frame traveling with the unperturbed wave. The rows show the perturbed solution at $t = 0$, $t = 250,000T$ and $t = 1,000,000T$, where $T = 2\pi/c = 28.09599$ is the time required for $\eta_0(x - ct)$ to traverse its wavelength. The effect of the initial perturbation is difficult to discern from η_0 in the top row of figure 6. At $t = 250,000T$, the perturbation has grown large enough to be visible in the figure, yielding small ripples in the troughs and regular subharmonic variation in the heights of the wave crests. The third row

($t = 1,000,000T$) shows the long-time evolution using the linear problem. Unlike the second row, these graphs do not represent the nonlinear dynamics of the water wave surface. Rather, since the perturbation has grown to several orders of magnitude larger than the profile $\eta_0(x)$, the third panel in effect shows the eigenfunction profile.

These results show that low-amplitude Wilton ripples are remarkably stable. With $\epsilon = 1.244 \times 10^{-6}$, which already deviates substantially from a sinusoidal wave profile (recall figure 2), the seeded wave can travel hundreds of thousands of wavelengths before losing coherence. Since $\mathrm{Re}(\lambda)$ decreases rapidly as $\epsilon \to 0$ (recall figure 5), this effect is even more pronounced at smaller amplitude. The two larger-amplitude waves studied in detail in figures 2, 3 and 4 are much less stable, with multiple unstable branches of eigenvalue curves and larger values of $\mathrm{Re}(\lambda)$, though still small compared to $1/T$.

4. Conclusion

Using numerical techniques similar to those in (Deconinck & Oliveras 2011) and (Deconinck & Trichtchenko 2014), as well as those introduced in (Wilkening & Yu 2012), we compute periodic traveling wave solutions of the full water wave problem (1a-d) including the effects of surface tension. We focus specifically on solutions whose small-amplitude limits are fully resonant, the so-called Wilton ripples. We present the first computation of the stability spectra of these solutions, providing an overview of the different types of instabilities to which they are susceptible. The resonance condition allows for a collision of six eigenvalues which was not present in non-resonant gravity-capillary waves. The smaller-amplitude resonant waves are found to be nearly spectrally stable, maintaining coherence while travelling hundreds of thousands of wavelengths. For larger-amplitude resonant waves, new types of instabilities are observed, manifesting themselves as nested structures and Benjamin-Feir-like instabilities present in shallow water waves. More comprehensive studies of these solutions and their instabilities will be presented in (Trichtchenko *et al.* 2015).

This work was supported in part by the National Science Foundation through grant NSF-DMS-1008001 (BD), by the EPSRC under grant EP/J019569/1 and by NSERC (OT), and by the Director, Office of Science, Computational and Technology Research, U.S. Department of Energy under contract number DE-AC02-05CH11231 (JW). Any opinions, findings, and conclusions or recommendations expressed in this material are those of the authors and do not necessarily reflect the views of the funding sources.

REFERENCES

Akers, B. & Gao, W. 2012 Wilton ripples in weakly nonlinear model equations. *Commun. Math. Sci.* **10** (3), 1015–1024.

Benjamin, T. B. 1967 Instability of periodic wavetrains in nonlinear dispersive systems. *Proc. Roy. Soc. (London) Ser. A* **299**, 59–76.

Benjamin, T. B. & Feir, J. E. 1967 The disintegration of wave trains on deep water. *J. Fluid Mech.* **27**, 417–430.

Craig, W. & Sulem, C. 1993 Numerical simulation of gravity waves. *Journal of Computational Physics* **108** (1), 73–83.

Curtis, C. W. & Deconinck, B. 2010 On the convergence of Hill's method. *Maths. of Computation* **79**, 169–187.

Deconinck, B. & Kutz, J. N. 2006 Computing spectra of linear operators using the Floquet-Fourier-Hill method. *Journal of Comp. Physics* **219**, 296–321.

Deconinck, B. & Oliveras, K. 2011 The instability of periodic surface gravity waves. *J. Fluid Mech.* **675**, 141–167.

Deconinck, B. & Trichtchenko, O. 2014 Stability of periodic gravity waves in the presence of surface tension. *Eur. J. Mech. B Fluids* **46**.

Haupt, S. E. & Boyd, J. P. 1988 Modeling nonlinear resonance: a modification to the Stokes' perturbation expansion. *Wave Motion* **10** (1), 83–98.

Henderson, D. M. & Hammack, J. L. 1987 Experiments on ripple instabilities. part 1. resonant triads. *J. Fluid Mech* **184**, 15–41.

Hislop, P. D. & Sigal, I. M. 1996 *Introduction to spectral theory*, *Applied Mathematical Sciences*, vol. 113. New York: Springer-Verlag, with applications to Schrödinger operators.

Johnson, M. A & Zumbrun, K. 2012 Convergence of Hill's method for nonselfadjoint operators. *SIAM Journal on Numerical Analysis* **50** (1), 64–78.

Jones, M.C.W. 1992 Nonlinear stability of resonant capillary-gravity waves. *Wave Motion* **15**, 267–283.

Jones, M.C.W. 1996 Evolution equations and stability results for finite-depth Wilton ripples. *International Journal of Non-Linear Mechanics* **31**, 41–57.

Kawahara, T. 1972 Oscillatory solitary waves in dispersive media. *J. Phys. Soc. Jpn.* **33**, 1015–1024.

Longuet-Higgins, M. S. 1978*a* The instabilities of gravity waves of finite amplitude in deep water. I. Superharmonics. *Proc. Roy. Soc. London Ser. A* **360**, 471–488.

Longuet-Higgins, M. S. 1978*b* The instabilities of gravity waves of finite amplitude in deep water. II. Subharmonics. *Proc. Roy. Soc. London Ser. A* **360**, 489–505.

MacKay, R. S. & Saffman, P.G. 1986 Stability of water waves. *Proc. R. Soc. London A* **406**, 115–125.

McGoldrick, L. F. 1970*a* An experiment on second-order capillary gravity resonant wave interactions. *Journal of Fluid Mechanics* **40**, 251–271.

McGoldrick, L. F. 1970*b* On Wilton's ripples: a special case of resonant interactions. *Journal of Fluid Mechanics* **42**, 193–200.

McGoldrick, L. F. 1971 On the rippling of small waves: a harmonic nonlinear nearly resonant interaction. *Journal of Fluid Mechanics* **52**, 725–751.

McLean, J. W. 1982 Instabilities of finite-amplitude water waves. *J. Fluid Mech.* **114**, 315–330.

Sethian, J. A. & Wilkening, J. 2004 A numerical model of stress driven grain boundary diffusion. *J. Comput. Phys.* **193** (1), 275–305.

Stokes, G. G. 1847 On the theory of oscillatory waves. *Mathematical and Physical Papers* **1**, 197–229.

Trichtchenko, O., Deconinck, B. & Wilkening, J. 2015 The instabilities of near-resonant and resonant periodic travelling gravity waves in the presence of surface tension. *In preparation* .

Vanden-Broeck, J.-M. 2010 *Gravity-Capillary Free-Surface Flows*. Cambridge University Press, Cambridge.

Vasan, V. & Deconinck, B. 2013 The Bernoulli boundary condition for traveling water waves. *Appl. Math. Lett.* **26** (4), 515–519.

Whitham, G. B. 1967 Non-linear dispersion of water waves. *J. Fluid Mech.* **27**, 399–412.

Wiggins, S. 1990 *Introduction to applied nonlinear dynamical systems and chaos*. Springer.

Wilkening, J. & Yu, J. 2012 Overdetermined shooting methods for computing standing water waves with spectral accuracy. *Computational Science & Discovery* **5** (1), 014017.

Wilton, J.R. 1915 On ripples. *Philosophical Magazine Series 6* **29** (173), 688–700.

Zakharov, V. E. 1968 Stability of periodic waves of finite amplitude on the surface of a deep fluid. *J. Appl. Mech. Tech. Phys.* **9**, 190–194.